Nonequilibrium Quantum Phase Transition in a Hybrid Atom-Optomechanical System

Niklas Mann,[1] M. Reza Bakhtiari,[1] Axel Pelster,[2] and Michael Thorwart[1]
[1]*I. Institut für Theoretische Physik, Universität Hamburg, Jungiusstraße 9, 20355 Hamburg, Germany*
[2]*Physics Department and Research Center OPTIMAS, Technische Universität Kaiserslautern, Erwin-Schrödinger Straße 46, 67663 Kaiserslautern, Germany*

(Received 26 October 2017; published 8 February 2018)

We consider a hybrid quantum many-body system formed by a vibrational mode of a nanomembrane, which interacts optomechanically with light in a cavity, and an ultracold atom gas in the optical lattice of the out-coupled light. The adiabatic elimination of the light field yields an effective Hamiltonian which reveals a competition between the force localizing the atoms and the membrane displacement. At a critical atom-membrane interaction, we find a nonequilibrium quantum phase transition from a localized symmetric state of the atom cloud to a shifted symmetry-broken state, the energy of the lowest collective excitation vanishes, and a strong atom-membrane entanglement arises. The effect occurs when the atoms and the membrane are nonresonantly coupled.

DOI: 10.1103/PhysRevLett.120.063605

Hybrid quantum systems combine complementary fields of physics, such as solid-state physics, quantum optics, and atom physics, in one setup. Recently, a hybrid atom-optomechanical system [1] has been realized experimentally [2] in which a single mechanical mode of a nanomembrane in an optical cavity is optically coupled to a far distant cloud of cold ^{87}Rb atoms residing in the optical potential of the out-coupled standing wave of the cavity light. When displaced, the membrane experiences the radiation pressure force of the cavity light, and in the bad-cavity limit, the field follows the membrane displacement adiabatically. This modulates the light phase, which leads to a shaking of the atom gas in the lattice. The nanomechanical motion of the membrane then couples nonresonantly to the collective motion of the atoms. The aim is twofold [1–7]: The gas can cool the nanomembrane, and emergent phenomena of the correlated quantum many-body system are of interest [8–17].

State-of-the-art optomechanics [3–6] is nowadays able to realize optical feedback cooling [18,19] of the mechanical oscillator to its quantum-mechanical ground state [20,21]. Yet the resolved sideband limit allows ground-state cooling only if the oscillator frequency exceeds the photon loss rate in the cavity [22–24]. Hence, cooling a macroscopic *low-frequency* nanomembrane close to its ground state is so far not possible. One promising alternative [1,7] is to utilize an ultracold atom gas, which has been demonstrated recently [2] by sympathetic cooling down to 650 mK. Current investigations aim toward a coherent state transfer of robust quantum entanglement [15].

Apart from cooling the nanomembrane, an interesting fundamental feature is the collective quantum many-body behavior of the hybrid system. For instance, the atom-atom interaction can in principle be coherently modulated by the backaction of the cavity light on the nanooscillator. By this, a long-range interaction emerges which resembles that of a dipolar Bose-Einstein condensate (BEC) [25]. In fact, a simpler hybrid quantum many-body system has also been implemented in the form of a BEC in an optical lattice inside a transversely pumped optical cavity. A Dicke quantum phase transition between a normal phase and a self-organized super-radiant phase occurs [26–30]. Moreover, optical bistability [31,32], a roton-type softening in the atomic dispersion relation [26,33–35], and optomechanical Bloch oscillations [36] have been uncovered. Similar effects occur also for polarizable and thermal particles in a cavity at finite temperature [37–39].

In this Letter, motivated by recent experiments [2,10], we study a hybrid atom-optomechanical setup in the form of a "membrane in the middle" cavity [1,2,8–11]; see Fig. 1. Importantly, the light-mediated coupling between the atoms and the membrane is nonresonant here. We include the full lattice potential and also the atomic interaction in the gas on the mean-field level. The numerical solution of the generalized Gross-Pitaevskii equation confirms the validity of an analytic approach based on a Gaussian condensate profile. Tuning the atom-membrane coupling by changing the laser intensity, a nonequilibrium quantum phase transition (NQPT) occurs between a localized symmetric state and a

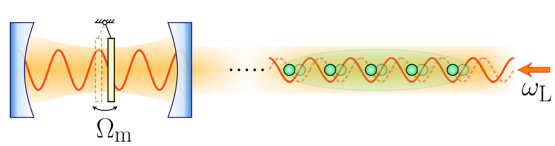

FIG. 1. Sketch of the hybrid system. A nanomechanical membrane in an optical cavity is optically coupled to the vibrational motion of a distant atom gas.

symmetry-broken quantum many-body state with a shifted cloud-membrane configuration. It is fueled by the competition of the lattice, trying to localize the atoms at the minima, and the membrane displacement which tries to shake the atoms. Near the quantum critical point, the energy of the lowest collective excitation mode vanishes, and the order parameter of the symmetry-broken state becomes nonzero, leading to a substantial atom-membrane entanglement. The mode softening is accompanied by a roton-type bifurcation of the decay rate of the collective eigenmodes. Indeed, an instability and collective self-oscillations of a coupled atom-membrane device have been reported recently [10].

Model.—We consider a single mechanical mode of a nanomembrane with frequency Ω_m placed in a low-finesse optical cavity. The outcoupled light forms an optical lattice in which a BEC is placed. In a quasistatic picture, a finite displacement of the membrane changes the position of the lattice sites, leading to a linear displacement force on the atoms, which induces transitions to higher motional bands. A backaction of the atomic motion on the membrane is induced by a displacement of their center-of-mass position, which, again, redistributes the photons in the propagating beams. Consequently, the light field inside the cavity changes, which alters the radiation pressure on the membrane. To achieve a sizable atom-membrane coupling, the typical energy scale of the BEC has to match the membrane frequency. This can be controlled by the light intensity which determines the lattice depth. The setup is sketched in Fig. 1 and modeled by a standard Hamiltonian, which describes the atom-membrane coupling directly [1,40]. In the bad-cavity limit, strong photon dissipation allows us to adiabatically eliminate the light field in a Born-Markov approximation [1], which yields the effective Hamiltonian

$$H = \int dz \Psi^\dagger(z)\left[-\omega_R\partial_z^2 + V\sin^2(z) + \frac{g}{2}\Psi^\dagger(z)\Psi(z)\right]\Psi(z) + \Omega_\mathrm{m} a^\dagger a - \lambda(a^\dagger + a)\int dz \Psi^\dagger(z)\sin(2z)\Psi(z). \quad (1)$$

Here, $\omega_R = \omega_L^2/2m$ is the recoil frequency of an atom with mass m, V is the optical lattice depth, and ω_L is the laser frequency. The last term describes the effective atom-membrane coupling with strength λ. Here, $a(a^\dagger)$ and $\Psi(\Psi^\dagger)$ are the bosonic annihilation (creation) operators of the membrane and bosons. Moreover, we have introduced a local atom-atom interaction with strength g and neglected long-range interaction, which is generated by the photon field. This is justified when the laser frequency is far detuned from the closest atomic transition.

In the condensate regime, a large fraction of the atoms occupies the ground state. Here, we consider weakly interacting atoms that are also weakly coupled to the membrane. Thus, when $g, \lambda \ll \omega_R, \Omega_\mathrm{m}$, the field operator $\Psi(z)$ can be approximated by a complex function $\psi(z)$ according to $\Psi(z) \simeq \sqrt{N}\psi(z)$, where N denotes the number of atoms. To describe the dynamics, we use the mean-field Lagrangian density associated with the Hamiltonian and given in Eq. (S9) of Ref. [40] with the complex number $\langle a\rangle/\sqrt{N} = \alpha = \alpha' + i\alpha''$ and the volume $\mathcal{V}$. We restrict the problem to a single lattice site—i.e., $\int dz \to \int_{-\pi/2}^{\pi/2} dz$ and $\mathcal{V} = \pi$—and use periodic boundary conditions. Then, we describe the dynamics analytically with a Gaussian ansatz for the condensate wave function and, in parallel, solve the generalized Gross-Pitaevskii equation (GPE) without further approximation. The Euler-Lagrange equations yield

$$\begin{aligned} i\partial_t\psi &= [V\sin^2(z) - \omega_R\partial_z^2 + gN|\psi|^2 - 2\sqrt{N}\lambda\alpha'\sin(2z)]\psi, \\ i\partial_t\alpha &= (\Omega_\mathrm{m} - i\gamma)\alpha - \sqrt{N}\lambda\int dz \sin(2z)|\psi|^2, \end{aligned} \quad (2)$$

where we have introduced a phenomenological damping of the mechanical mode with a rate γ. This is due to finite losses caused by the clamping of the membrane as well as the radiation pressure.

From Eq. (2), we see that the two potential contributions $V\sin^2(z)$ and $\sqrt{N}\lambda(\alpha + \alpha^*)\sin(2z)$ can dynamically compete with each other, depending on the backaction of the membrane on the atoms, and thus on the collective behavior of the atoms. This competition yields to the formation of two different stable phases and a NQPT. It is manifest in a change of the center-of-mass position of the condensate, or the membrane displacement, equivalently. Formal similarities to the NQPT in the Dicke-Hubbard model [29,30] exist. There, however, a self-organized symmetry-broken checkerboard lattice occupation is formed above a critical transverse pump strength which induces a coherent light scattering into the longitudinal cavity mode [26,27]. In the present setup, the spatial periodicity of the optical lattice remains unchanged, and symmetry breaking is manifest in a global collective shift of the potential.

To describe a realistic physical setup, we consider a membrane with $\Omega_\mathrm{m} = 100\omega_R$, which corresponds to a frequency of several hundred kHz. Here, we describe the condensate profile by a Gaussian [41]

$$\psi(z,t) = \left(\frac{1}{\pi\sigma(t)^2}\right)^{1/4} e^{-\{[z-\zeta(t)]^2/2\sigma(t)^2\} + i\kappa(t)z + i\beta(t)z^2} \quad (3)$$

with a time-dependent width $\sigma(t)$, centered at the position $\zeta(t)$, and the corresponding phases $\beta(t)$ and $\kappa(t)$. For an accurate description, we consider $V \gtrsim 10\omega_R$ and $Ng \ll V$. To find the equations of motion of these variational parameters, we determine the lowest cumulants of the condensate probability distribution whose dynamics is described by the generalized GPE [Eq. (2)]. Thus, we multiply the first line of Eq. (2) by $\psi^*(z)(z-\zeta)$ and integrate over z; and likewise, we multiply the same line by $\psi^*(z)[(z-\zeta)^2 - \sigma^2/2]$ and integrate over z. This yields four linearly independent equations for the variational parameters, two of which are $\dot{\zeta} = 2\omega_R(\kappa + 2\beta\zeta)$ and $\dot{\sigma} = 4\omega_R\beta\sigma$. With these, we find

$$\begin{aligned} 2\Omega_{\mathrm{m}}^{-1}[\ddot{\alpha}' + 2\gamma\dot{\alpha}'] &= -\partial_{\alpha'}E, \\ (2\omega_R)^{-1}\ddot{\zeta} &= -\partial_\zeta E, \\ (4\omega_R)^{-1}\ddot{\sigma} &= -\partial_\sigma E, \end{aligned} \tag{4}$$

where the potential energy $E = -\int dz\mathcal{L}|_{\dot{\alpha}=\dot{\psi}=0}$ reads

$$E = \frac{gN}{\sqrt{8\pi}\sigma} - \frac{V\sqrt{1-\mathcal{S}^2} + 4\sqrt{N}\lambda\alpha'\mathcal{S}}{2\exp(\sigma^2)} + \frac{\omega_R}{2\sigma^2} + \tilde{\Omega}_{\mathrm{m}}\alpha'^2, \tag{5}$$

with the effective frequency $\tilde{\Omega}_{\mathrm{m}} = \Omega_{\mathrm{m}} + \gamma^2/\Omega_{\mathrm{m}}$. Importantly, we have defined the order parameter $\mathcal{S} = \sin(2\zeta)$ of the NQPT, which describes the center-of-mass position of the condensate.

Quantum phase transition in the mean-field regime.—Due to the mechanical damping, the combined system will eventually equilibrate. The steady state is characterized by those values $\alpha'_0, \sigma_0, \mathcal{S}_0$ which minimize the potential energy functional $E(\alpha', \sigma, \mathcal{S})$. Indeed, by setting all time derivatives in Eq. (4) to zero and using Eq. (5), we find the relation $\sqrt{N}\lambda\mathcal{S}_0 = \tilde{\Omega}_{\mathrm{m}}\alpha'_0 e^{\sigma_0^2}$, so that the equilibrium width σ_0 and order parameter $\mathcal{S}_0$ solve the coupled equations $(1-\mathcal{S}_0^2)^{1/2}[\omega_R + gN\sigma_0/\sqrt{8\pi}] = V\sigma_0^4 e^{-\sigma_0^2}$ and $\mathcal{S}_0[N\lambda^2(1-\mathcal{S}_0^2)^{1/2} - N\lambda_{c,V}^2 e^{\sigma_0^2}] = 0$, with $N\lambda_{c,V}^2 = \tilde{\Omega}_{\mathrm{m}}V/4$.

For a qualitative understanding of the role of increasing λ, we define the potential energy surface as a function of a single variable; i.e., either σ or $\mathcal{S}$ (or α'). For instance, $E(\sigma) \equiv E[\alpha'_0(\sigma), \sigma, \mathcal{S}_0(\sigma)]$ exhibits only a single minimum for $\sigma > 0$. Interestingly enough, as a function of the control parameter λ, the energy $E(\mathcal{S})$ has either one stable state or two minima. This is visualized by the normalized potential energy surface $\epsilon(\mathcal{S}, \lambda) = [E(\mathcal{S}) - E(\mathcal{S}_0)]/\max\{E(\mathcal{S}) - E(\mathcal{S}_0)\}$ in Fig. 2(a). The red curve marks the configuration of minimal energy $\epsilon(\mathcal{S}_0, \lambda) = 0$. There exists a critical coupling λ_c, such that for smaller values $\lambda < \lambda_c$, the energy surface forms a single potential well, whereas for $\lambda > \lambda_c$, it becomes a double-well potential with a local maximum at $\mathcal{S} = 0$.

The order parameter as a function of the atom-membrane coupling λ is shown in Fig. 2(b) for different values of the lattice depth. The solid curves show the results of the analytical approach, whereas the dashed lines refer to the numerical solution of the full GPE. For small values λ, the condensate is symmetrically located around the lattice minima $\zeta_0 = j\pi$ with $j \in \mathbb{Z}$, so the order parameter vanishes, $\mathcal{S}_0 = 0$. Consequently, the membrane displacement $\alpha'_0 \sim \mathcal{S}_0$ vanishes. The NQPT then occurs at a critical coupling λ_c, which follows from solving the implicit equation

$$\omega_R + \frac{gN}{\sqrt{8\pi}}\sqrt{2\ln\frac{\lambda_c}{\lambda_{c,V}}} = 4V\left(\frac{\lambda_{c,V}}{\lambda_c}\ln\frac{\lambda_c}{\lambda_{c,V}}\right)^2. \tag{6}$$

Above λ_c, the atoms start to move away from the positions $j\pi$ to the displaced lattice minima. The order parameter becomes finite: $\mathcal{S}_0 = \pm\Theta(\lambda - \lambda_c)\sqrt{1 - (\lambda_{c,V}/\lambda)^4 e^{2\sigma_0^2}}$ and can be scaled to a single curve as shown in the inset of Fig. 2(b). The condensate width $\sigma_0(\lambda)$ is shown in Fig. 2(c) and is independent of λ below λ_c, whereas it decreases in good approximation with $\sim 1/\sqrt{\lambda}$ above λ_c. In accordance with an expansion of the energy surface with respect to the order parameter, all these observables show within our mean-field treatment that the hybrid system undergoes a second-order NQPT. In contrast to the super-radiant phase of the Dicke phase transition, a global displacement of the lattice minima and membrane is observed, and the lattice periodicity is not changed.

Collective excitation modes.—Solving the complete set of equations of motion (4) is challenging, but their linearized forms give already an insight into the collective excitation energies. We consider small deviations from the stationary state $[\alpha'_0, \sigma_0, \mathcal{S}_0(\text{or } \zeta_0)]$ in the forms $\alpha'(t) = \alpha'_0 + \delta\alpha'(t)$, $\sigma(t) = \sigma_0 + \delta\sigma(t)$, and $\zeta(t) = \zeta_0 + \delta\zeta(t)$, and we linearize the equations of motion in the deviations. We find Eq. (S10) in the Supplemental Material [40].

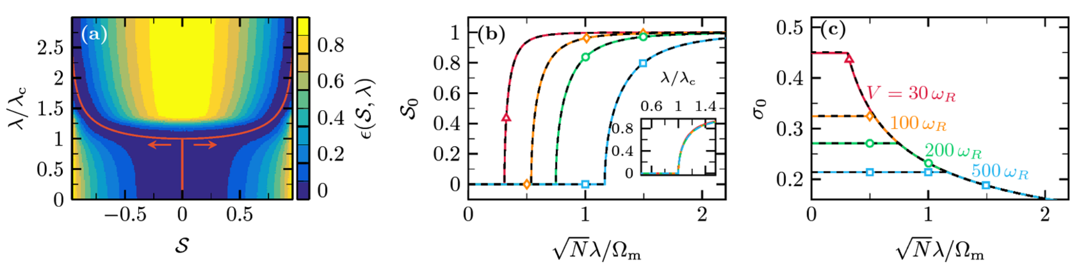

FIG. 2. (a) Normalized potential energy surface $\epsilon(\mathcal{S}, \lambda)$ as a function of $\mathcal{S}$ and λ for $V = 200\omega_R$. The red line indicates the minimum $\epsilon(\mathcal{S}_0, \lambda) = 0$. (b) Positive value of $\mathcal{S}_0$ and (c) condensate width σ_0 as a function of λ for different values V as indicated in (c). The dashed curves show the GPE results for comparison. The inset in (b) shows the order parameter $\mathcal{S}_0$ as a function of λ/λ_c for which all data points collapse to a single curve. For all panels, we have used $g = 0$, $\Omega_{\mathrm{m}} = 100\omega_R$, and $\gamma = 20\omega_R$.

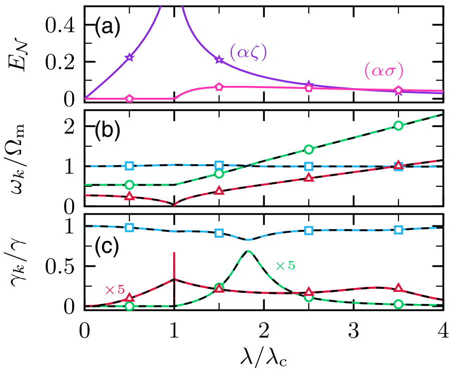

FIG. 3. (a) Atom-membrane entanglement by the logarithmic negativity of the ground state ($\gamma = 0$) between membrane and either atom displacement (purple) or condensate width (pink). (b) Frequencies of collective excitations. (c) Decay rates of the collective eigenmodes (some curves are scaled by the factors indicated). Curves in blue, green, and red correspond to the membrane mode, the condensate width mode, and the atomic displacement excitation, respectively. The dashed curves show the GPE results. The parameters are $V = 200\omega_R$, $\Omega_{\rm m} = 100\omega_R$, $\gamma = 20\omega_R$, and $g = 0$.

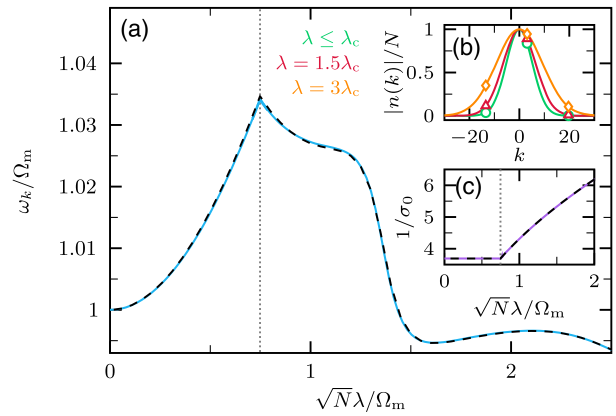

FIG. 4. (a) Membrane excitation frequency and (b) momentum distribution $|n(k)|$ of the atoms in a single well. (c) Width of $|n(k)|$ in dependence of λ. The dotted vertical line indicates λ_c. The parameters are $V = 200\omega_R$, $\Omega_{\rm m} = 100\omega_R$, $\gamma = 20\omega_R$, and $g = 0$.

Interestingly, the oscillation frequencies also indicate the NQPT. Below λ_c, the bare frequency $\omega_\zeta = \sqrt{4\omega_R V e^{-\sigma_0^2/2}}$ of the ζ mode is independent of λ, whereas above λ_c, it grows linearly in λ according to $\omega_\zeta = \sqrt{4\omega_R V e^{-\sigma_0^2}}\lambda/\lambda_c$.

In addition, the eigenmodes can be determined [40] from the differential equations in the vector-matrix form $\dot{\boldsymbol{x}} = \boldsymbol{M}\boldsymbol{x}$. The eigenvalues $\nu_k = i\omega_k - \gamma_k$ of $\boldsymbol{M}$ define the eigenfrequencies ω_k and the decay rates γ_k. Likewise, we estimate the eigenmodes via the GPE by considering small deviations from the ground state according to $\psi(z,t) = e^{i\mu t}[\psi_0(z) + \delta\psi(z,t)]$ and $\alpha(t) = \alpha_0 + \delta\alpha(t)$. Linearization with respect to the deviations results in a differential equation of the form $\dot{\boldsymbol{w}}(z) = \boldsymbol{M}_{\rm GP}\boldsymbol{w}(z)$, where the eigenvalues of $\boldsymbol{M}_{\rm GP}$ provide the eigenfrequencies and the decay rates [40].

The eigenfrequencies of the collective excitations without interatomic collisions are shown in Fig. 3(b), and the corresponding decay rates in Fig. 3(c), as a function of the atom-membrane coupling strength. [Figs. S2(b) and S2(d) [40] show zooms to the critical region.] The dashed lines show the frequency (rate) calculated in the GPE approach, whereas the solid lines refer to the analytical results. Approaching the critical coupling, the lowest excitation frequency (red, triangles) in Fig. 3(b) decreases with a roton-type behavior according to $\sim\sqrt{1 - \lambda^2/\lambda_c^2}$. At the same time, the corresponding decay rate increases to a maximum at λ_c. In a narrow range $\Delta\lambda \simeq 0.1\omega_R$ around λ_c, a bifurcation of the decay rate can be observed, whereas the lowest excitation frequency is constantly zero. Such a behavior is well known from atomic ensembles with long-range interactions [34,35,42,43] which, in the present case, are mediated by the membrane. Indeed, adiabatically eliminating the membrane mode introduces a long-range interaction potential that takes the form $G(z,z') = G_0 \sin(2z)\sin(2z')$ with $G_0 = -2\lambda^2/\tilde{\Omega}_{\rm m}$. Moreover, the ground state ($\gamma = 0$) of the collective modes is a three-mode squeezed state; see Eq. (S14) [40]. This generates a strong atom-membrane entanglement close to the critical point. This behavior is manifest in a rising logarithmic negativity $E_{\mathcal{N}}$ [44–46] at the critical point, which is shown in Fig. 3(a). For $\gamma = 0$, it diverges there, while it is expected to be finite for $\gamma > 0$ [44]. Finally, we note that although all figures refer to the case $g = 0$, no qualitative differences occur for weakly interacting atoms [40].

Experimental realization.—An experimental observation is possible in existing setups; e.g., in Ref. [11]. Current optical lattices with $V \simeq 2000\omega_R$ readily achieve a resonant coupling [40]; i.e., $\omega_\zeta \simeq \Omega_{\rm m}$, with $\sqrt{N}\lambda \simeq 3\omega_R$. The fact that the effective atom-membrane coupling in our scheme does not have to be resonant facilitates the realization. For instance, by loading the atoms in a lattice with $V = 30\omega_R$, $\sqrt{N}\lambda_c \simeq 30\omega_R$ can be reached by tuning the laser power and cavity finesse [1]. Moreover, an independent tuning of λ can be achieved by applying a second laser which is slightly misaligned with the first one and which generates an optical lattice of the same periodicity but shifted by $\pi/2$. The membrane eigenfrequency shown in Fig. 4(a) can readily be measured spectroscopically with a relative precision of much below 1%, so that the cusp at λ_c will be clearly resolvable. In addition, the NQPT can also be detected via the momentum distribution of the atoms shown in Fig. 4(b), together with its width for varying λ in Fig. 4(c). Below λ_c, the width is constant, while it increases monotonically for $\lambda > \lambda_c$.

Conclusions.—We have shown that a hybrid atom-optomechanical system possesses a nonequilibrium quantum phase transition between phases of different collective behavior. Based on a Gross-Pitaevskii-like mean-field approach, the steady state of an ultracold atomic condensate in an optical lattice, whose motion is nonresonantly coupled to a single mechanical vibrational mode of a spatially distant membrane, has been analyzed. The coupling between both parts occurs via the light field of a common laser. Below the critical effective atom-membrane coupling λ_c, the atoms in the combined atom-membrane ground state are symmetrically distributed around their lattice minima. At the quantum critical point, a nonequilibrium quantum phase transition to a symmetry-broken state occurs in which the atomic center-of-mass and membrane displacements are all either positive or negative. Near the NQPT, the lowest excitation mode shows roton-type characteristics in the excitation frequency, a mode softening and a bifurcation of the decay rate, accompanied by a strong atom-membrane entanglement. A potential application could be to measure the atom momentum fluctuations nondestructively by measuring the fluctuations of the membrane displacement.

This work was supported by the Deutsche Forschungsgemeinschaft (N. M.), by DFG Collaborative Research Center 928 "Light-induced dynamics and control of correlated quantum systems" (M. R. B.), and by DFG Collaborative Research Center/TransRegio 185 "Open system control of atomic and photonic matter" (A. P.). We thank Christoph Becker, Alexander Schwarz, and Hai Zhong for useful discussions on experimental setups.

[1] B. Vogell, K. Stannigel, P. Zoller, K. Hammerer, M. T. Rakher, M. Korppi, A. Jöckel, and P. Treutlein, Phys. Rev. A **87**, 023816 (2013).
[2] A. Jöckel, A. Faber, T. Kampschulte, M. Korppi, M. T. Rakher, and P. Treutlein, Nat. Nanotechnol. **10**, 55 (2015).
[3] M. Aspelmeyer, T. J. Kippenberg, and F. Marquardt, Rev. Mod. Phys. **86**, 1391 (2014).
[4] T. J. Kippenberg and K. J. Vahala, Science **321**, 1172 (2008).
[5] I. Favero and K. Karrai, Nat. Photonics **3**, 201 (2009).
[6] M. Aspelmeyer, S. Gröblacher, K. Hammerer, and N. Kiesel, J. Opt. Soc. Am. B **27**, A189 (2010).
[7] B. Vogell, T. Kampschulte, M. T. Rakher, A. Faber, P. Treutlein, K. Hammerer, and P. Zoller, New J. Phys. **17**, 043044 (2015).
[8] M. Wallquist, K. Hammerer, P. Rabl, M. Lukin, and P. Zoller, Phys. Scr. **T137**, 014001 (2009).
[9] D. Hunger, S. Camerer, M. Korppi, A. Jöckel, T. Hänsch, and P. Treutlein, C.R. Phys. **12**, 871 (2011).
[10] A. Vochezer, T. Kampschulte, K. Hammerer, and P. Treutlein [Phys. Rev. Lett. (to be published)].
[11] H. Zhong, G. Fläschner, A. Schwarz, R. Wiesendanger, P. Christoph, T. Wagner, A. Bick, C. Staarmann, B. Abeln, K. Sengstock, and C. Becker, Rev. Sci. Instrum. **88**, 023115 (2017).
[12] D. Meiser and P. Meystre, Phys. Rev. A **73**, 033417 (2006).
[13] C. Genes, D. Vitali, and P. Tombesi, Phys. Rev. A **77**, 050307 (2008).
[14] H. Ian, Z. R. Gong, Yu-xi Liu, C. P. Sun, and F. Nori, Phys. Rev. A **78**, 013824 (2008).
[15] K. Hammerer, M. Aspelmeyer, E. S. Polzik, and P. Zoller, Phys. Rev. Lett. **102**, 020501 (2009).
[16] K. Hammerer, M. Wallquist, C. Genes, M. Ludwig, F. Marquardt, P. Treutlein, P. Zoller, J. Ye, and H. J. Kimble, Phys. Rev. Lett. **103**, 063005 (2009).
[17] M. Paternostro, G. De Chiara, and G. M. Palma, Phys. Rev. Lett. **104**, 243602 (2010).
[18] P. H. Cohadon, A. Heidmann, and M. Pinard, Phys. Rev. Lett. **83**, 3174 (1999).
[19] D. Kleckner and D. Bouwmeester, Nature (London) **444**, 75 (2006).
[20] J. D. Teufel, T. Donner, D. Ji, J. W. Harlow, M. S. Allman, K. Cicak, A. J. Sirois, J. D. Whittaker, K. W. Lehnert, and R. W. Simmonds, Nature (London) **475**, 359 (2011).
[21] J. Chan, T. P. Mayer Alegre, A. H. Safavi-Naeini, J. T. Hill, A. Krause, S. Gröblacher, M. Aspelmeyer, and O. Painter, Nature (London) **478**, 89 (2011).
[22] W. Neuhauser, M. Hohenstatt, P. Toschek, and H. Dehmelt, Phys. Rev. Lett. **41**, 233 (1978).
[23] F. Marquardt, J. P. Chen, A. A. Clerk, and S. M. Girvin, Phys. Rev. Lett. **99**, 093902 (2007).
[24] A. Schliesser, R. Rivière, G. Anetsberger, O. Arcizet, and T. J. Kippenberg, Nat. Phys. **4**, 415 (2008).
[25] T. Lahaye, C. Menotti, L. Santos, M. Lewenstein, and T. Pfau, Rep. Prog. Phys. **72**, 126401 (2009).
[26] D. Nagy, G. Szirmai, and P. Domokos, Eur. Phys. J. D **48**, 127 (2008).
[27] C. Maschler, I. B. Mekhov, and H. Ritsch, Eur. Phys. J. D **46**, 545 (2008).
[28] K. Baumann, C. Guerlin, F. Brennecke, and T. Esslinger, Nature (London) **464**, 1301 (2010).
[29] M. R. Bakhtiari, A. Hemmerich, H. Ritsch, and M. Thorwart, Phys. Rev. Lett. **114**, 123601 (2015).
[30] J. Klinder, H. Keßler, M. R. Bakhtiari, M. Thorwart, and A. Hemmerich, Phys. Rev. Lett. **115**, 230403 (2015).
[31] S. Gupta, K. L. Moore, K. W. Murch, and D. M. Stamper-Kurn, Phys. Rev. Lett. **99**, 213601 (2007).
[32] S. Ritter, F. Brennecke, K. Baumann, T. Donner, C. Guerlin, and T. Esslinger, Appl. Phys. B **95**, 213 (2009).
[33] B. Öztop, M. Bodyuh, Ö. E. Müsecaplıoğlu, and H. E. Türeci, New J. Phys. **14**, 085011 (2012).
[34] R. Mottl, F. Brennecke, K. Baumann, R. Landig, T. Donner, and T. Esslinger, Science **336**, 1570 (2012).
[35] J. Léonard, A. Morales, P. Zupancic, T. Donner, and T. Esslinger, Science **358**, 1415 (2017).
[36] H. Keßler, J. Klinder, B. Prasanna Venkatesh, C. Georges, and A. Hemmerich, New J. Phys. **18**, 102001 (2016).
[37] J. K. Asbóth, P. Domokos, H. Ritsch, and A. Vukics, Phys. Rev. A **72**, 053417 (2005).
[38] W. Lu, Y. Zhao, and P. F. Barker, Phys. Rev. A **76**, 013417 (2007).
[39] T. Salzburger and H. Ritsch, New J. Phys. **11**, 055025 (2009).
[40] See Supplemental Material at http://link.aps.org/supplemental/10.1103/PhysRevLett.120.063605 for more

details on the effective Hamiltonian and its Lagrangian density, the eigenmode analysis of the collective excitations, the experimental realization, the role of the atom interactions, and the atoms' momentum distribution.

[41] H. Al-Jibbouri and A. Pelster, Phys. Rev. A **88**, 033621 (2013).

[42] L. Santos, G. V. Shlyapnikov, and M. Lewenstein, Phys. Rev. Lett. **90**, 250403 (2003).

[43] S. Giovanazzi and D. H. J. O'Dell, Eur. Phys. J. D **31**, 439 (2004).

[44] G. Adesso, A. Serafini, and F. Illuminati, Phys. Rev. A **70**, 022318 (2004).

[45] D. Nagy, G. Szirmai, and P. Domokos, Phys. Rev. A **84**, 043637 (2011).

[46] M. Eghbali-Arani and V. Ameri, Quantum Inf. Process. **16**, 47 (2017).